Seasonal Variation in Precipitation Patterns to the Global Ocean: An Analysis of the GPCP Version 2 Data Set

Jinchun Yuan[1] and **Richard Miller**[2]

[1]NRC Postdoctoral Fellow, NASA, Earth Science Applications Directorate, Stennis Space Center, MS 39529

[2]NASA, Earth Science Applications Directorate, Stennis Space Center, MS 39529

Jinchun Yuan
Tel. (228) 688-3522
Fax: (228) 688-1777
Email: jinchun.yuan@ssc.nasa.gov

Richard Miller
Tel. (228) 688-1904
Fax: (228) 688-1777
Email: richard.miller@ssc.nasa.gov

Abstract

Precipitation affects the thermohaline circulation, chemical mass balance, and primary productivity of surface ocean waters. An analysis of temporal and spatial variation of oceanic precipitation was conducted on the Global Precipitation Climatology Project (GPCP) version 2 data set, a monthly 2.5 x 2.5° latitude-longitude gridded data set for the period 1979 to 1999. While the precipitation patterns observed are generally similar to those reported in previous climatologies, new features and greater detail of global precipitation were revealed from our analysis of the GPCP data set. High precipitation was observed in the inter-tropical convergence zone (ITCZ), the South Pacific convergence zone (SPCZ), and the storm tracks in the North Pacific and Atlantic Oceans. Low precipitation was observed in the Polar regions and in the subtropics of the East Pacific, East Atlantic, and the Southeast and Northwest Indian Ocean. The spatial coverage of these high and low precipitation regions changed through the year. A strong seasonal cycle of precipitation was observed for the Northern and the Southern Hemispheres. The area-weighted mean precipitation increased from a minimum of ~2 mm d^{-1} in February to a maximum of ~5 mm d^{-1} in August in the Northern Hemisphere and from a minimum of ~2.5 mm d^{-1} in September to a maximum of ~3.5 mm d^{-1} in March in the Southern Hemisphere. Similar seasonal cycles of precipitation were observed for each ocean basin. Global precipitation also varied significantly with both latitude and longitude, with a latitudinal maximum at 56°S, 39°S, 4°S, 6°N, 39°N, and 56°N, and a longitudinal maximum over each ocean. The seasonal varying precipitation patterns are a foundation for evaluating the effect of wet deposition on ocean circulation, flux of chemical species, and its effect on marine ecosystems.

Introduction

Precipitation to the ocean affects processes ranging from global thermohaline circulation [*Broecker et al.*, 1990; *Zancker et al.*, 1994] and mass balance of chemical species [*Zika and Saltzman*, 1982; *Cooper et al.*, 1987; *Martin et al.*, 1991; *Church et al.*, 1991; *Willey et al.*, 2000; *Yuan and Shiller*, 2000], to marine primary productivity [*Paerl*, 1985; *Paerl et al.*, 1999]. Due to the limitations of traditional sampling and measurement methods, the temporal and spatial variations of precipitation over the ocean are poorly known [*Penman*, 1970; *Lvovitch*, 1973]. As a result, the effects of freshwater input on ocean circulation, chemical fluxes, and biological processes have long been estimated using bulk precipitation calculated for entire oceans or specific regions [*Holland*, 1978; *Broecker et al.*, 1990; *Berner and Berner*, 1996]. These bulk numbers are derived mainly by three methods: (1) shipboard measurements [*Jaeger, 1983*]; (2) estimates based on limited rain gauge observations on oceanic islands [for a review see: *Huffman et al.*, 1995; and *Xie and Arkin*, 1995]; and (3) differences between estimated total evaporation and measured continental precipitation [*Holland*, 1978]. Recently, satellite observed infrared (IR) and microwave (MW) radiances have been used to retrieve precipitation information over many parts of the world, including the ocean [*Arkin and Meisner*, 1987; *Arkin and Ardanuy*, 1989; *Janowiak and Arkin*, 1991; *Arkin et al.*, 1994; *King et al.*, 1995; *Joyce and Arkin*, 1997; *Kummerow et al.*, 1998].

Each method of precipitation measurement has its advantages and shortcomings. Rain gauges offer direct measurement of precipitation, but only at point locations. Satellite remote sensing offers better spatial coverage, but suffers from poor temporal

coverage or systematic bias [*Huffman et al.*, 1997]. Numerical models provide relatively high quality precipitation estimates for mid- and high latitudes where rain gauges and satellite coverage are sometimes lacking [*Arpe*, 1991]. Therefore, to generate high-quality precipitation data with global coverage, one must combine results from all of these methods [*Arkin and Janowiak*, 1991; *Huffman et al.*, 1997; *Xie and Arkin*, 1997].

Two schemes were applied in generating precipitation data sets with global coverage. Xie and Arkin [1997] and the Global Precipitation Climatology Project (GPCP) [*Huffman et al.*, 1997] combined rain gauge observations, satellite estimates, and numerical model output to generate global monthly 2.5° x 2.5° latitude-longitude gridded precipitation data sets. A comparison study indicates that these two data sets depict similar global precipitation patterns with some minor differences, and the GPCP data set is more accurate [*Gruber et al.*, 2000]. We present here an analysis of the seasonal and spatial variation of precipitation to the ocean using the GPCP data set. We hope to lay a foundation for further studies of the effect of precipitation on ocean processes based on these newly available data sets.

Data and Methods

The GPCP Version 2 (V2) data set, a monthly global precipitation (2.5° x 2.5° grid) from January 1979 to November 1999, was used for this study. Data are not available in high latitudes for some months, such that analyses for these regions are based on 18 years of precipitation data.

Area-weighted mean precipitation was calculated for the ocean and the globe. The area, S, of the 2.5° x 2.5° grid is calculated as:

$$S = \frac{2\pi Rh\Delta\gamma}{360} \quad (1)$$

where $\Delta\gamma$ is the size of the longitude grid (= 2.5), R is the radius of the earth, and h is given by:

$$h = R(\sin\alpha - \sin\beta) \quad (2)$$

where α and β are the starting and ending latitudes of the grid.

The seasonal variation of precipitation to the ocean was fitted to a cosine function as follows:

$$P = A\cos(\frac{2\pi}{B}T + T_0) + P_0 \quad (3)$$

where P and P_0 are precipitation and seasonal mean precipitation, T is time, and A, B, and T_0 are amplitude, period, and phase constant of precipitation fluctuation, respectively.

Results

Average annual precipitation to the ocean

In general, oceanic regions received more precipitation than the continents (Figure 1). The majority of the ocean received about 100 to 150 cm y^{-1} precipitation, compared to less than 100 cm y^{-1} received by most parts of the continents. Lower

latitudes received more precipitation than higher latitudes. The precipitation patterns of the ocean can be viewed as several dry and wet regions within a relatively high precipitation background of 100 to 150 cm y^{-1}.

A dry region, defined as annual precipitation below 50 cm, was observed in each ocean basin (Figure 1). In the North Indian Ocean, the dry region was located at the western part of the basin, with its north-south extension decreasing toward the east. Apart from the dry region in the North Indian Ocean, all the dry regions were located mainly in the subtropics at the eastern basin of each ocean with the north-south extension increasing eastward.

Wet regions (precipitation > 200 cm y^{-1}) were found mainly in the low latitudes (Figure 1). The major wet region fell within the inter-tropical convergence zone (ITCZ) and extended from the eastern equatorial Indian Ocean, through the equatorial Pacific Ocean, and to the eastern equatorial Atlantic Ocean. A brief interruption of the ITCZ wet region was observed near the east coast of Africa, where precipitation fell below 100 cm y^{-1}. Additionally, the ITCZ wet region extended northward in the East Indian Ocean and southward in the West Pacific to the South Pacific convergence zone (SPCZ). Finally, two wet regions were seen in the storm tracks of the Northwest Pacific and Atlantic Oceans.

Seasonal variation of oceanic precipitation patterns

During the studied period, each ocean contained dry (precipitation < 2 mm d^{-1}) and wet (precipitation > 4 mm d^{-1}) regions that varied on a monthly basis (Figures 2 to 5).

Pacific Ocean

From January to March (Figure 2), the subpolar and subtropical dry regions expanded gradually in the Northeast Pacific, while the temperate wet region retreated from the Northeast Pacific and expanded southwestward. At the same time, the ITCZ wet region expanded southward and split into two wet belts in March. In the South Pacific, the SPCZ wet region expanded southeastward, while the subtropical dry region shrank.

From April to June (Figure 3), the subpolar and subtropical dry regions merged to cover the majorities of the Northeast Pacific. In May and June, the temperate wet region expanded further southwestward, joining the ITCZ wet region. The ITCZ wet belts recombined in June. In the South Pacific, the SPCZ wet region shrank, while the subtropical dry region expanded westward.

From July to September (Figure 4), the subpolar and subtropical dry regions reduced in size and began to separate. The temperate wet region expanded eastward to reach North America. In the South Pacific, the subtropical dry region expanded further west to reach Australia, resulting in the separation of the ITCZ and SPCZ wet regions.

From October to December (Figure 5), the temperate wet region expanded to occupy the major part of the North Pacific. The subtropical dry region expanded westward to China, separating the temperate and ITCZ wet regions. In the South Pacific,

the ITCZ and SPCZ wet regions reconnected with the retreat of the subtropical dry region.

Atlantic Ocean

From January to March (Figure 2), the temperate wet and subtropical dry regions occupied most of North Atlantic with the precipitation intensity of the wet region decreasing in the northeast. In the South Atlantic, the subtropical wet region expanded southeastward, while the subtropical dry region decreased in size.

From April to June (Figure 3), the subpolar and subtropical dry regions expanded to occupy the majority of the North Atlantic Ocean; the temperate wet region was correspondingly reduced. In the South Atlantic, the subtropical dry region expanded westward to South America and the subtropical wet region retreated southward.

From July to September (Figure 4), the temperate wet region expanded northeastward and southwestward, with a corresponding retreat of subpolar and subtropical dry regions. In the South Atlantic Ocean, the spatial coverage of the subtropical dry and the subtropical wet regions remained relatively consistent.

From October to December (Figure 5), the temperate wet region expanded in the northeast and retreated slightly from the western Atlantic. The subtropical dry region shifted westward to reach North America. In the South Atlantic, the subtropical wet region expanded northward with the retreat of the subtropical dry region.

Indian Ocean

From January to March (Figure 2), the subtropical dry region covered the majority of the North Indian Ocean. The ITCZ wet region covered the equatorial and tropical Southern Indian Ocean, with its precipitation intensity decreasing. In the South Indian Ocean, the subtropical dry region expanded westward.

From April to June (Figure 3), the subtropical dry region retreated from the Northeast and North-Central Indian Ocean, and expanded southward across the west equatorial Indian Ocean. The ITCZ wet region expanded into the Northeastern Indian Ocean. The precipitation intensity in the ITCZ wet region increased during this period, but the maximum precipitation was found in the Northeast Indian Ocean, not at the equator. The subtropical dry region of the South Indian Ocean expanded further westward and northwestward. By June, the two subtropical dry regions of the Indian Ocean were connected.

From July to September (Figure 4), the combination of the subtropical dry regions covered the northwest, equatorial, south tropical, and south subtropical Indian Ocean. The ITCZ wet region and its northward extension covered the major part of the equatorial and the Northeast Indian Ocean, and its precipitation intensity decreased.

From October to December (Figure 5), the connection between the subtropical dry regions of the Indian Ocean gradually diminished. In the North Indian Ocean, the

subtropical dry region expanded eastward to cover both the Northwest and the Northeast Indian Ocean. In the South Indian Ocean, the subtropical dry region retreated eastward.

ITCZ and Polar Frontal Zone

For both the Pacific and Atlantic Oceans, the precipitation intensity in the ITCZ wet regions varied seasonally. The maximum rainfall shifted through the year from the west end of the ITCZ between January and April, to the east end of the ITCZ between May and September, and to the central part of the ITCZ between October and December.

Different precipitation patterns were observed in the Polar front of the Arctic and the Antarctic (Figures 1-5). On an annual basis, between 100 to 150 cm y^{-1} of precipitation was observed across the Antarctic front, while a similar level of precipitation was observed only in limited regions across the Arctic front, namely over the North Pacific and the North Atlantic Oceans. Most of the Arctic front receives less than 100 cm y^{-1} precipitation. In some Arctic front regions, such as North America, North Asia, and North Europe (Figure 1), precipitation even falls below 50 cm y^{-1}.

The precipitation in the Antarctic Polar Front Zone (APFZ) varied significantly with season. It increased from January to April, and decreased from May to December (Fig. 2 to 5). The APFZ qualifies as a wet region in April and May, a dry region in December; and it is a combination of wet and dry regions in other months.

Seasonal variation of area-weighted mean precipitation

As reported in the previous section, ocean precipitation patterns varied seasonally. However, seasonal variation was not obvious in area-weighted means of global precipitation (Figure 6 a). Regression analysis indicated that the area-weighted mean precipitation to the Northern (Figure 6 b) and Southern (Figure 6 c) Hemispheres each varied seasonally (eq. 3) during the 21 years studied. Because there was a phase difference in seasonal variation of precipitation between the two hemispheres (Figure 6 b and c), global variation appears to cancel out (Figure 6a).

This regression analysis revealed four primary features. First, the seasonal mean of area-weighted precipitation was almost identical for the Northern (2.74 mm d^{-1}) and Southern (2.71 mm d^{-1}) Hemispheres. Second, the period of seasonal cycle was approximately one year (12.1 and 12.4 months, for the Northern and Southern Hemispheres, respectively). Third, the amplitudes of seasonal fluctuation of precipitation were 0.64 and 0.68 mm d^{-1} for the Northern and Southern Hemispheres, respectively. And finally, maximum precipitation occurred in August-September for the Northern Hemisphere and in February-March for the Southern Hemisphere.

A regression analysis (eq. 3) was also conducted on the area-weighted mean precipitation of each ocean basin (Table 1). Again, there was an apparent seasonal variation of precipitation for either the northern or southern portion of a particular ocean, while the phase differences of these variations tended to cancel out seasonal variation for each ocean as a whole.

Regression analysis of the area-weighted mean precipitation to the ocean showed three trends (Table 1). First, seasonal mean of area-weighted precipitation varied from a low of 3.00 mm d^{-1} for the South Indian Ocean to a high of 4.17 mm d^{-1} for the North Atlantic Ocean. The seasonal mean of area-weighted precipitation to the ocean (3.00 to 4.17) was thus higher than that of the global oceans (2.74 and 2.71). Consequently, the observed mean precipitation to the ocean was higher than that to the continents. Second, the period of seasonal cycle of precipitation to the ocean is approximately one year (from 11.3 to 14.1 months). Third, the amplitude of seasonal fluctuations of precipitation to global oceans varied from 0.59 to 1.82 mm d^{-1}.

Latitudinal and Longitudinal Variation of Area-Weighted Mean Global Precipitation

Latitudinal and longitudinal variation of precipitation was also calculated from the area-weighted mean global precipitation. From south to north, six precipitation maxima and seven precipitation minima were observed (Figure 7). Precipitation also varied significantly with longitude (Figure 8). Three major peaks in precipitation were observed at approximately 90°, 160°, and 310°. These peaks correspond to the East Indian, the West Pacific, and the West Atlantic Oceans, respectively. This longitudinal variation of precipitation is expected because oceans, particularly western regions of oceans, generally receive more precipitation than continents (see above).

Discussion

Global precipitation pattern

Although our analysis of the GPCP V2 data set yielded precipitation patterns similar to that reported previously [*Penman*, 1970; *Jaeger*, 1983; *Legates and Willmott*, 1990], several new features and greater detail were apparent. Traditionally, precipitation patterns of continents are derived from rain gauge measurements, while those of oceanic regions are defined with sparse ship data [*Jaeger*, 1983; *Legates and Willmott*, 1990]. Our analysis was based on 21 years of the GPCP V2 data set, which took advantage of several satellite remote sensing techniques and offered improved spatial coverage and temporal resolution. Detailed analysis of seasonal variations of precipitation patterns of the oceans was therefore possible.

Previously, wet deposition fluxes of chemical species were estimated on ocean basin and annual scales *[Duce et al.; 1991]*. We contend that given the temporal and spatial variability of oceanic precipitation presented here and the short resident time of some trace and reactive species [*Yuan and Shiller, 2001*], wet chemical fluxes of reactive chemical species and their biological effects should be reevaluated.

The widely quoted trend of latitudinal variation in net precipitation is characterized by three maxima at 55°S, 3°N, and 50°N and two minima at 15°S and 23°N [*Peixoto and Kettani*, 1973]. Instead of three maxima, our analysis showed six maxima. Perhaps the maxima observed in this study were decompositions of those previously reported (Figure 7). Although this trend may be altered by taking into account

evaporation, which follows sea surface temperature in decreasing away from the equator, it is unlikely that evaporation alone can mask the newly apparent maxima. Moreover, it should be noted that our analysis placed these maxima at slightly different latitudes than previously reported [*Peixoto and Kettani*, 1973].

Prior to this study, analysis of seasonal variations of precipitation for global land, global ocean, and the entire globe indicated that seasonal cycle was not clearly defined (Figure 15 of *Xie and Arkin*, 1997). We found that by treating the Northern and Southern Hemispheres separately, seasonal cycles were obvious for the globe (Figure 6) and the ocean (Table 1). Our analysis indicated that mean precipitation in the oceans of the Northern Hemisphere (3.89, 4.17, and 3.23 mm d^{-1}) is higher than that of the Southern Hemisphere (3.09, 3.67, and 3.00 mm d^{-1}). This is understandable since mean precipitation to the Northern and the Southern Hemispheres is almost identical, and continents, which occupy more area in the Northern Hemisphere, receive much less precipitation.

Additionally, the mean precipitation to the Atlantic (4.17 and 3.67 mm d^{-1}) is higher than that of the Pacific (3.89 and 3.09 mm d^{-1}) and Indian Oceans (3.23 and 3.00 mm d^{-1}). This is very interesting because it has been argued that there should be a net freshwater flux from the Atlantic to the Pacific and Indian Oceans [*Zancker et al.*, 1994]. If the mean precipitation calculated here is typical, either the evaporation from the Atlantic Ocean has to be significantly higher or river runoff significantly smaller than that of the Pacific and Indian Oceans to support the higher freshwater fluxes.

Ocean circulation and precipitation patterns

It appears that ocean circulation and precipitation patterns are partially correlated. Apart from high precipitation at the ITCZ, there are two main oceanic regions in the Northern Hemisphere that received high precipitation: one in the vicinity of the Gulf Stream in the Northwest Atlantic Ocean, and the other near the Kuroshio in the Northwest Pacific Ocean (Figure 1). In the Southern Hemisphere (Figure 1), three relatively wet regions are located near 30°S in the southwest regions of the Indian, Pacific, and Atlantic Oceans, respectively. All these wet regions are in the west ocean basins, where surface currents transport warm equatorial water to higher latitudes. Higher sea surface temperature should lead to higher vapor pressure and higher air temperature, and consequently higher precipitation. Therefore, ocean circulation patterns may be one of the causes of the observed precipitation patterns.

The different Polar fronts and the split ITCZ

There is a significant difference in the precipitation between the Polar front in the Arctic and the Antarctic (Figures 1-5). Between 100 to 150 cm y^{-1} of precipitation were observed across the Antarctic front, while a similar level of precipitation was observed only in limited regions across the Arctic front. This asymmetrical distribution of precipitation patterns may be related to the asymmetrical distribution of continents.

Basin scale split of the ITCZ was observed in the Pacific in March, April, and May (Figure 2 and 3). In the other months of the year, a split ITCZ was also observed but it was constrained to a small region in the West Pacific (Figure 2 to 5). A seasonal

split of the ITCZ has been reported previously [*Huffman et al.*; 1997; *Quartly et al.*, 2000].

Conclusions

Temporal and spatial variations of precipitation to the ocean were evaluated using a recently released GPCP V2 data set. Several wet regions, with precipitation in excess of 150 cm y^{-1}, and dry regions, with precipitation less than 50 cm y^{-1}, were identified. Higher precipitation was observed in the ITCZ, the SPCZ, and the storm tracks in the North Pacific and the North Atlantic. Lower precipitation was observed in the Polar regions, and in the subtropics of the East Pacific and East Atlantic, and in the subtropics of the Southeast and Northwest Indian Ocean. The spatial distribution of these wet and dry regions varied seasonally. Area-weighted mean precipitation for the Northern and Southern Hemispheres, as well as for each ocean basin, also varied seasonally. In the Northern Hemisphere, the minimum was in February and maximum was in August. In the Southern Hemisphere, the minimum was in September and the maximum was in March. Global precipitation varied significantly with both latitude and longitude, with a latitudinal maximum at 56°S, 39°S, 4°S, 6°N, 39°N, and 56°N, and a longitudinal maximum over each of the oceans. The temporal and spatial variations of precipitation patterns can be used to estimate fluxes of fresh water and chemical species to different oceanic regions, their seasonal variations, and their biological effects.

Acknowledgements

The authors wish to thank the NASA/Goddard Space Flight Center's Laboratory for Atmospheres for providing the GPCP V2 precipitation data. We would also like to thank Virginia Miller, Gregory Carter, and Carlos Del Castillo for useful comments and discussions. J. Yuan was supported by an NRC RA while at the NASA J. C. Stennis Space Center.

References

Arkin, P.A., and B.N. Meisner, The relationship between large-scale convective rainfall and cold cloud over the western hemisphere during 1982-84, *Monthly Weather Review*, *115* (1), 51-74, 1987.

Arkin, P.A., and P.E. Ardanuy, Estimating climate-scale precipitation from space: a review, *Journal of Climate*, *2* (11), 1229-1238, 1989.

Arkin, P., and J. Janowiak, Analysis of the global distribution of precipitation, *Dynamics of Atmospheres and Oceans*, *16*, 5-16, 1991.

Arkin, P.A., R. Joyce, and J.E. Janowiak, The estimation of global monthly mean rainfall using infrared satellite data: the GOES precipitation index (GPI), *Remote Sensing Reviews*, *11*, 107-124, 1994.

Arpe, K., The hydrological cycle in the ECMWF short-range forecasts, *Dynamics of Atmospheres and Oceans*, *16*, 33-60, 1991.

Berner, E.K., and R.A. Berner, *Global Environment: Water, Air, and Geochemical Cycles*, Prentice Hall, New Jersey, 1996.

Broecker, W.S., T.-H. Peng, J. Jouzel, and G. Russell, The magnitude of global fresh-water transports of importance to ocean circulation, *Climate Dynamics*, *4*, 73-79, 1990.

Church, T.M., J.M. Tramontano, D.M. Whelpdale, M.O. Andreae, J.N. Galloway, W.C. Keene, A.H. Knap, and J. J. Tokos, Atmospheric and precipitation chemistry over the North Atlantic Ocean: shipboard results, April-May 1984, *Journal of Geophysical Research*, *96* (D10), 18705-18725, 1991.

Cooper, W.J., E.S. Saltzman, and R.G. Zika, The contribution of rainwater to variability in surface ocean hydrogen peroxide, *Journal of Geophysical Research*, *92* (C3), 2970-2980, 1987.

Gruber, A., X. Su, M. Kanamitsu, and J. Schemm, The comparison of two merged rain gauge-satellite precipitation datasets, *Bulletin of the American Meterological Society*, *81* (11), 2631-2644, 2000.

Holland, H.D., *The Chemistry of The Atmosphere and Oceans*, John Wiely & Sons, New York, 1978.

Huffman, G.J., R.F. Adler, P. Arkin, A. Chang, R. Ferraro, A. Gruber, J. Janowiak, A. McNab, B. Rudolf, and U. Schneider, The global precipitation climatology project (GPCP) combined precipitation dataset, *Bulletin of the American Meterological Society*, *78* (1), 5-20, 1997.

Huffman, G.J., R.F. Adler, B. Rudolf, U. Schneider, and P.R. Keehn, Global precipitation estimates based on a technique for combining satellite-based estimates, rain gauge analysis, and NWP model precipitation information, *Journal of Climate*, *8*, 1284-1295, 1995.

Jaeger, L., Monthly and areal patterns of mean global precipitation. *Variations in the Global Water Budget*, A. Street-Perrott, M. Beran, and R. Ratcliffe, Eds., D. Reidel Publ. Co., Dordrecht, 129-140, 1983.

Janowiak, J.E., and P.A. Arkin, Rainfall variation in the tropics during 1986-1989, as estimated from observations of cloud-top temperature, *Journal of Geophysical Research*, *96*, 3359-3373, 1991.

Joyce, R., and P.A. Arkin, Improved estimates of tropical and subtropical precipitation using the GOES precipitation index, *Journal of Atmospheric and Oceanic Technology*, *14*, 997-1011, 1997.

King, P.W.S., W.D. Hogg, and P.A. Arkin, The role of visible data in improving satellite rain-rate estimates, *Journal of Applied Meteorology*, *34* (7), 1608-1621, 1995.

Kummerow, C., W. Barnes, T. Kozu, J. Shiue, and J. Simpson, The tropical rainfall measuring mission (TRMM) sensor package, *Journal of Atmospheric and Oceanic Technology*, *15* (3), 809, 1998.

Legates, D.R., and C.J. Willmott, Mean seasonal and spatial variability in gauge corrected global precipitation, *Int. J. Climatol.*, *10*, 111-127, 1990.

Lvovitch, M.I., The global water balance, *Trans. Amer. Geophys. Res.*, *90* (D3), 28-42, 1973.

Martin, J.H., R.M. Gordon, and S.E. Fitzwater, The case for iron, *Limnology and Oceanography*, *36* (8), 1793-1802, 1991.

Paerl, H.W., Enhancement of marine primary production by nitrogen-enriched acid rain, *Nature*, *315*, 747-749, 1985.

Paerl, H.W., J.D. Willey, M. Go, B.L. Peierls, J.L. Pinckney, and M.L. Fogel, Rain stimulation of primary production in western Atlantic Ocean waters: roles of different nitrogen sources and co-limiting nutrients, *Marine Ecology Progress Series*, *176*, 205-214, 1999.

Peixoto, J.P., and M.A. Kettani, The control of the water cycle, *Scientific American*, *228* (4), 46-61, 1973.

Penman, H.L., The water cycle, *Scientific American*, *223* (3), 99-108, 1970.

Quartly, G.D., M.A. Srokosz, and T.H. Guymer, Changes in oceanic precipitation during the 1997-1998 El Niño, *Geophysical Research Letters*, *27* (15), 2293-2296, 2000.

Willey, J.D., R.J. Kieber, M.S. Eyman, and G.B.A. Jr., Rainwater dissolved organic carbon: concentrations and global flux, *Global Biogeochemical Cycles*, *14* (1), 139-148, 2000.

Xie, P., and P. Arkin, Analysis of global monthly precipitation using gauge observations, satellite estimates, and numerical model predictions, *Journal of Climate*, *9*, 840-858, 1995.

Xie, P., and P.A. Arkin, Global precipitation: A 17 year monthly analysis based on gauge observation, satellite estimates, and numerical model outputs, *Bulletin of the American Meteorological Society*, *78* (11), 2539-2558, 1997.

Yuan, J., and A.M. Shiller, The variation of hydrogen peroxide in rainwater over the South and Central Atlantic Ocean, *Atmospheric Environment*, *34* (23), 3973-3980, 2000.

Yuan, J., and A. M. Shiller, The distribution of hydrogen peroxide in the southern and Central Atlantic Ocean, *Deep-Sea Research II*, *48* (13), 2947-2970, 2001.

Zancker, F., T.F. Stocker, and W.S. Broecker, Atmospheric freshwater fluxes and their effect on the global thermohaline circulation, *Journal of Geophysical Research*, *99* (C6), 12443-12457, 1994.

Zika, R.G., and E.S. Saltzman, H_2O_2 levels in rainwater collected in South Florida and the Bahama Islands, *Journal of Geophysical Research*, *87* (C7), 5015-5017, 1982.

Figure Captions

Figure 1. Average precipitation (cm y^{-1}) to the oceans based on 21 years of GPCP V2 data set.

Figure 2. Average precipitation (mm d^{-1}) to the oceans in January (top), February (middle), and March (bottom) based on 21 years of GPCP V2 data set.

Figure 3. Average precipitation (mm d^{-1}) to the oceans in April (top), May (middle), and June (bottom) based on 21 years of GPCP V2 data set.

Figure 4. Average precipitation (mm d^{-1}) to the oceans in July (top), August (middle), and September (bottom) based on 21 years of GPCP V2 data set.

Figure 5. Average precipitation (mm d^{-1}) to the oceans in October (top), November (middle), and December (bottom) based on 21 years of GPCP V2 data set.

Figure 6. Seasonal variation of area-weighted mean precipitation (mm d^{-1}) to the globe (a), the northern (b), and the southern (c) hemispheres. The solid line is a nonlinear fit of the precipitation. The mean precipitation is calculated from 21 years of GPCP V2 data set.

Figure 7. Latitudinal variation of area-weight mean precipitation (mm d^{-1}) to the globe based on 21 years of GPCP V2 data set.

Figure 8. Longitudinal variation of precipitation (mm d^{-1}) to the globe based on 21 years of GPCP V2 data set.

Table 1. Regression of the seasonal variation of global precipitation

Global Region	Maximum (month)	Minimum (month)	Amplitude (mm d^{-1})	Seasonal mean (mm d^{-1})	R^2
Northern Hemisphere Total	8-9	2-3	0.64	2.74	0.912
Southern Hemisphere Total	2-3	8-9	0.68	2.71	0.922
North Pacific Ocean	8-9	2-3	0.78	3.89	0.723
South Pacific Ocean	2-3	8-9	0.71	3.09	0.772
North Atlantic Ocean	7-8	2	1.42	4.17	0.831
South Atlantic Ocean	2	8-9	0.82	3.69	0.676
North Indian Ocean	7-8	1-2	1.82	3.23	0.654
South Indian Ocean	2-3	9-10	0.59	3.00	0.684

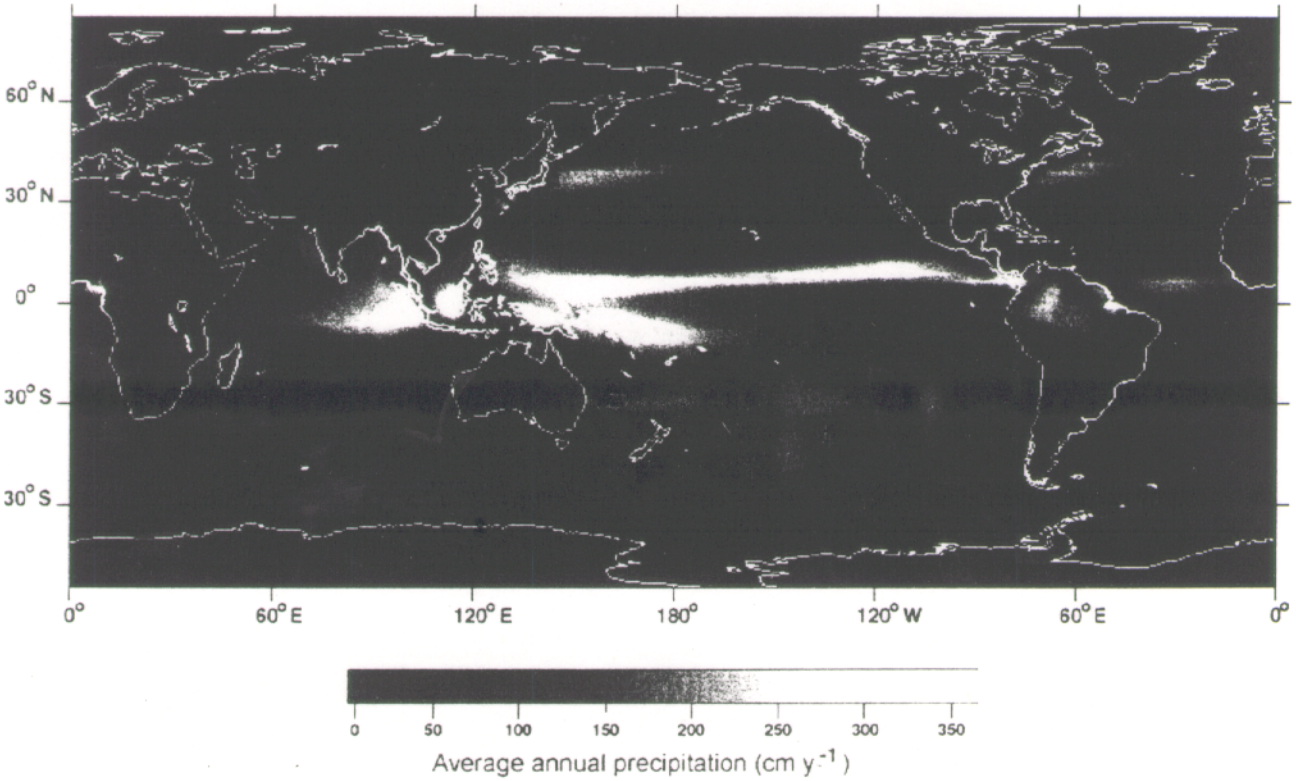
60° N
30° N
0°
30° S
30° S
0°
60° E
120° E
180°
120° W
60° E
0°
0
50
100
150
200
250
300
350
Average annual precipitation (cm y-1)

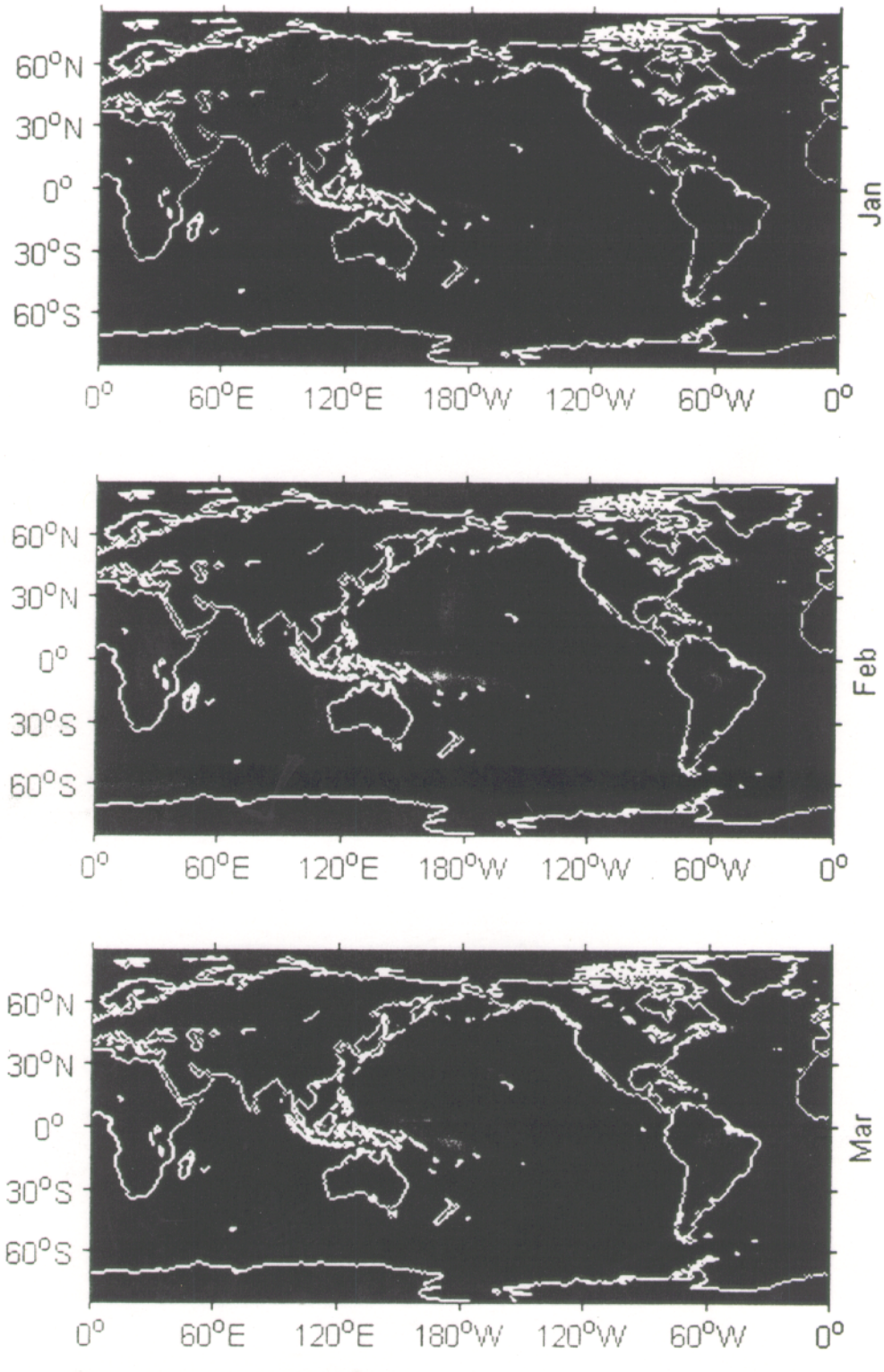
60°N
30°N
0°
30°S
60°S
0°
60°E
120°E
180°W
120°W
60°W
0°
Jan
Feb
Mar
0
2
4
6
8
10
12
14
16
18
20
Average monthly precipitation (mm d-1)

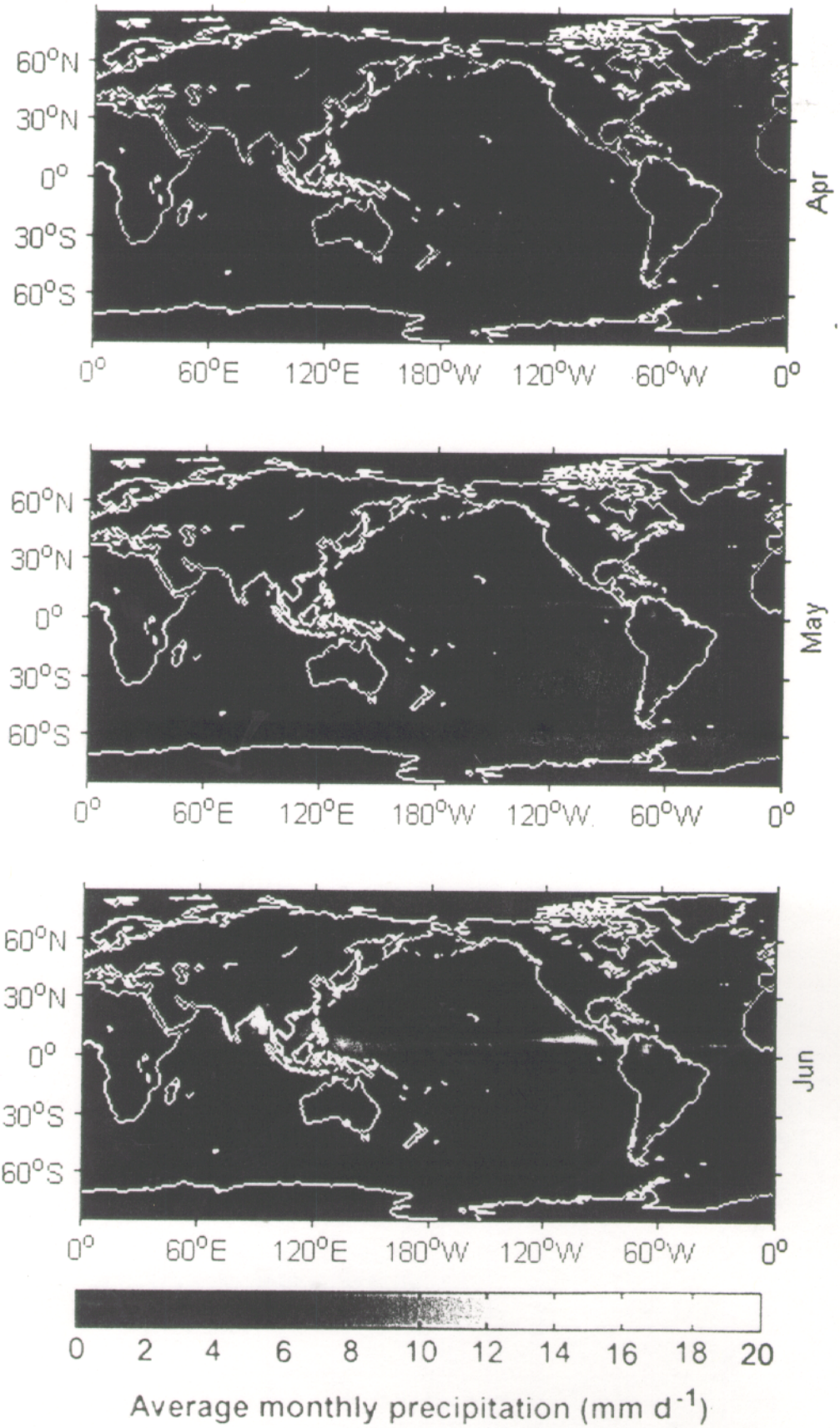
60°N
30°N
0°
30°S
60°S
0°
60°E
120°E
180°W
120°W
60°W
0°
Apr
May
Jun
0
2
4
6
8
10
12
14
16
18
20
Average monthly precipitation (mm d-1)

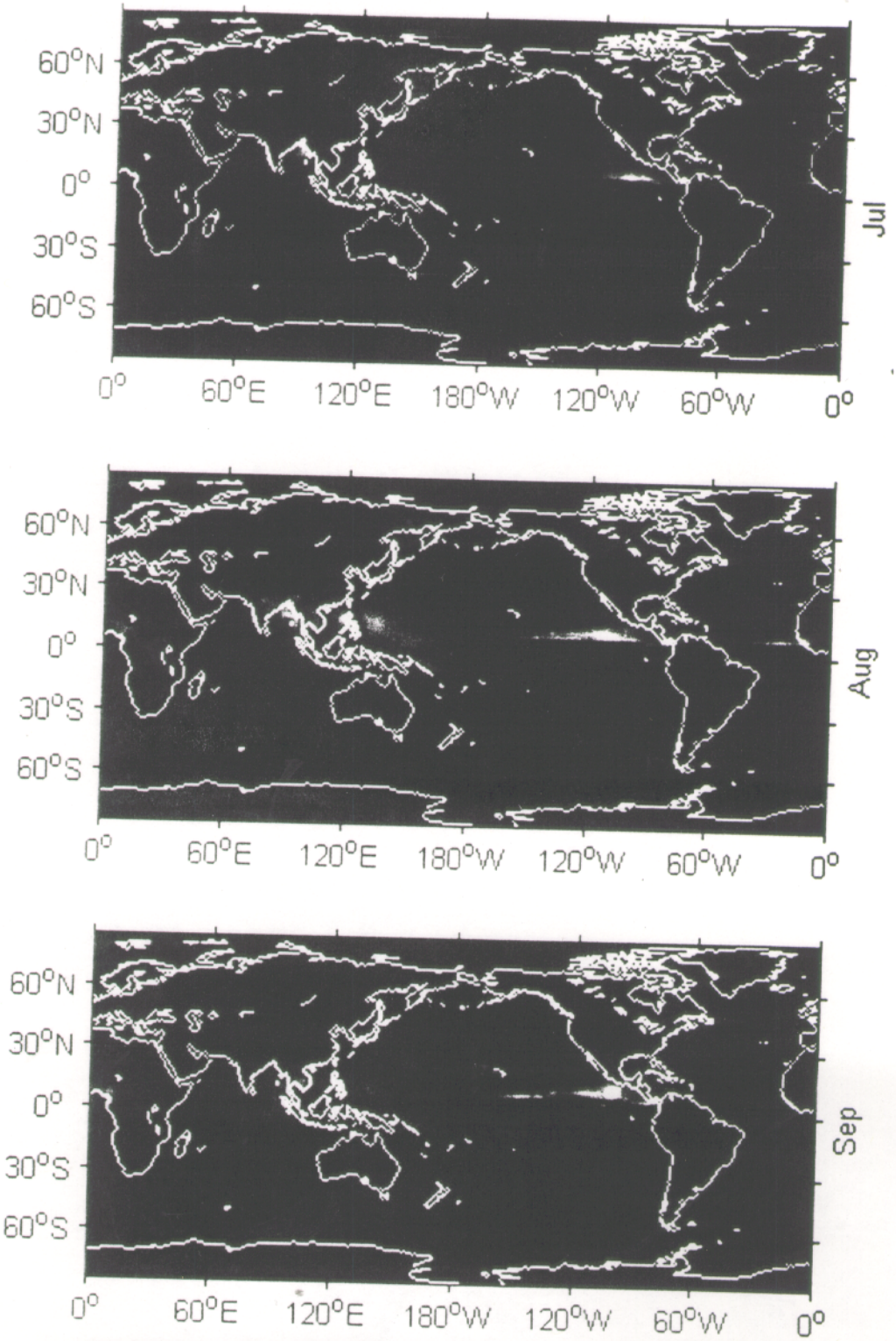
60°N
30°N
0°
30°S
60°S
0°
60°E
120°E
180°W
120°W
60°W
0°
Jul
Aug
Sep
0
2
4
6
8
10
12
14
16
18
20
Average monthly precipitation (mm d-1)

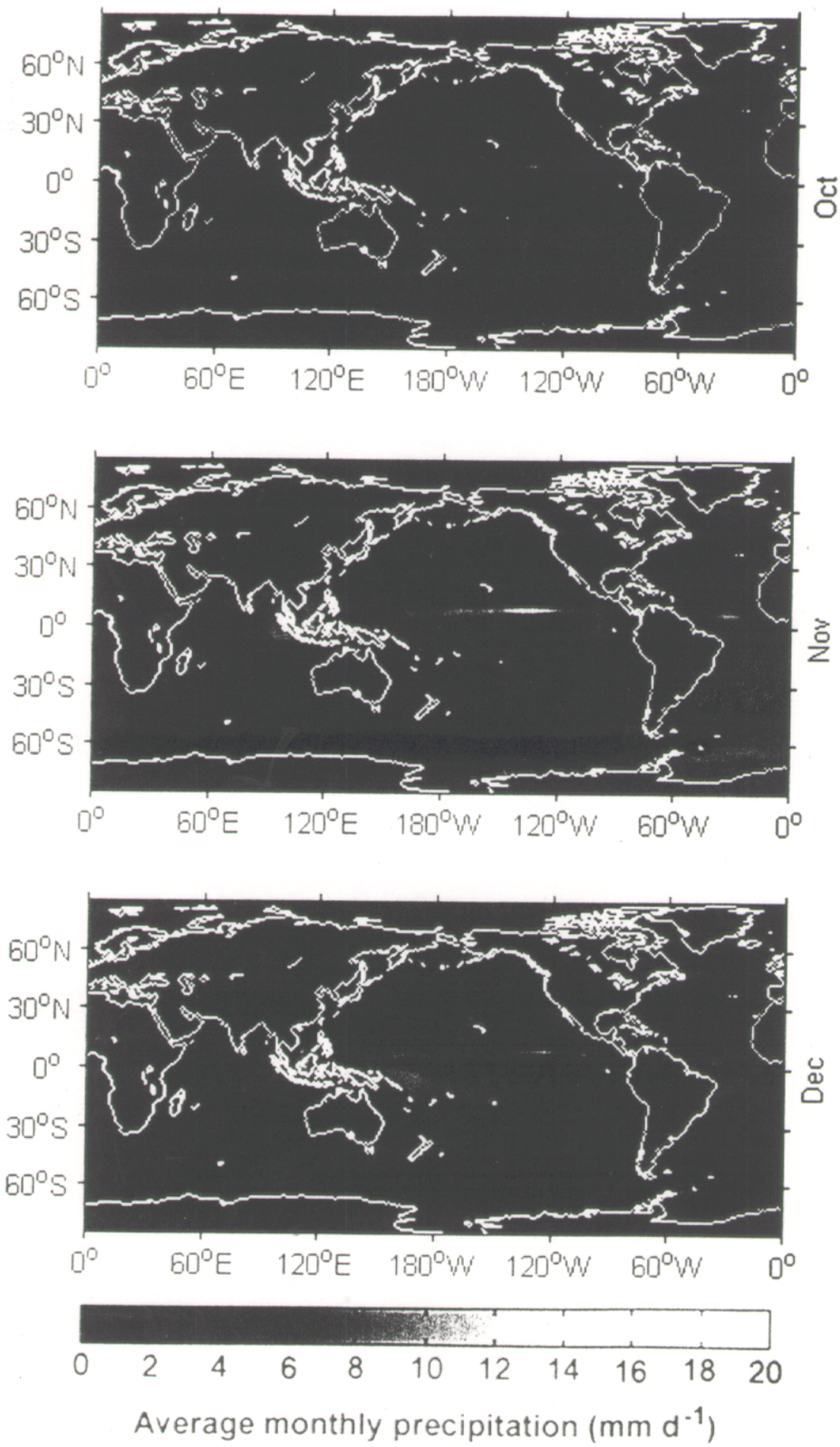
60°N
30°N
0°
30°S
60°S
0°
60°E
120°E
180°W
120°W
60°W
0°
Oct
Nov
Dec
0
2
4
6
8
10
12
14
16
18
20
Average monthly precipitation (mm d-1)

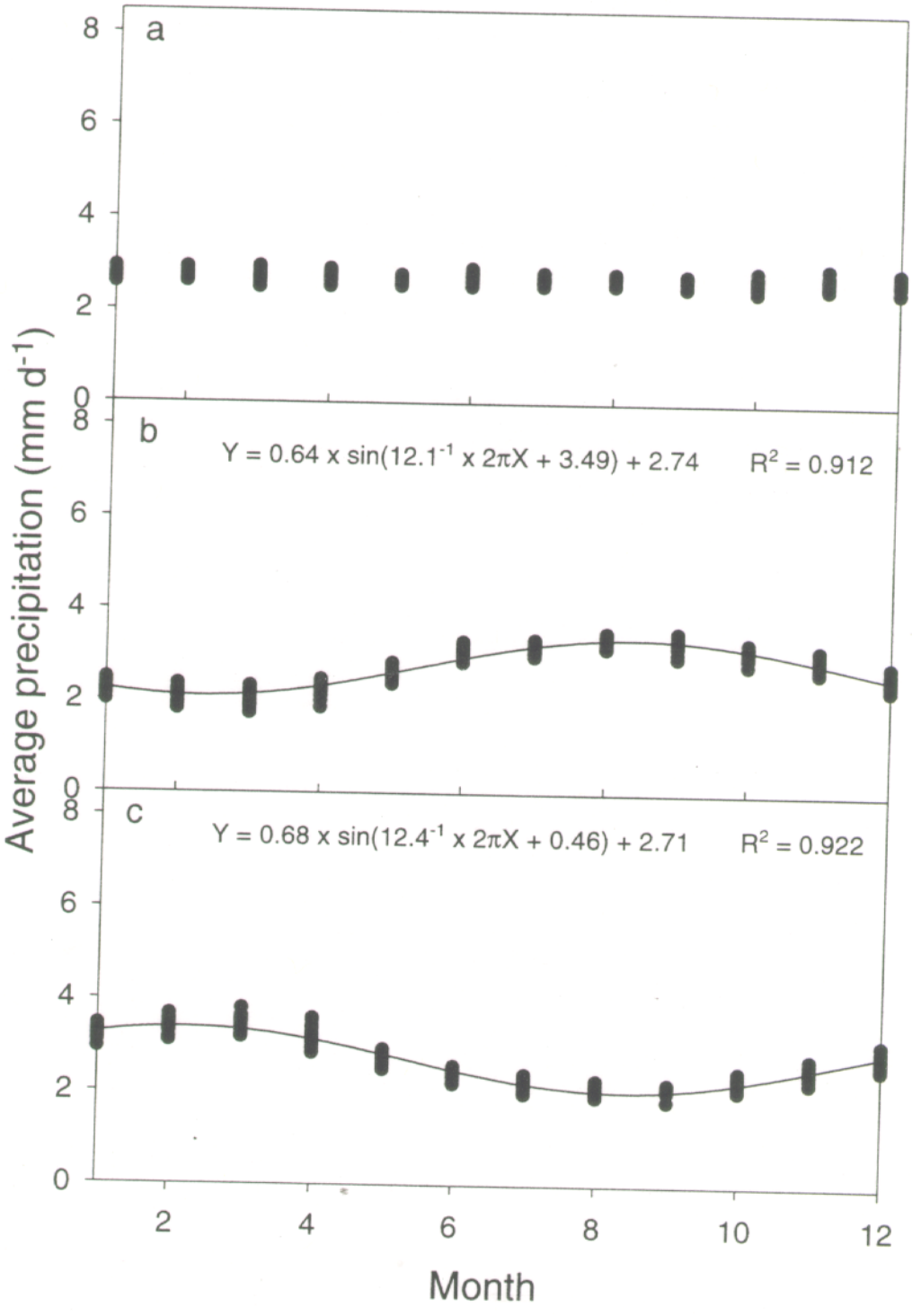
a
b
c
Y = 0.64 x sin(12.1-1 x 2πX + 3.49) + 2.74
R2 = 0.912
Y = 0.68 x sin(12.4-1 x 2πX + 0.46) + 2.71
R2 = 0.922
Average precipitation (mm d-1)
Month
0
2
4
6
8
10
12

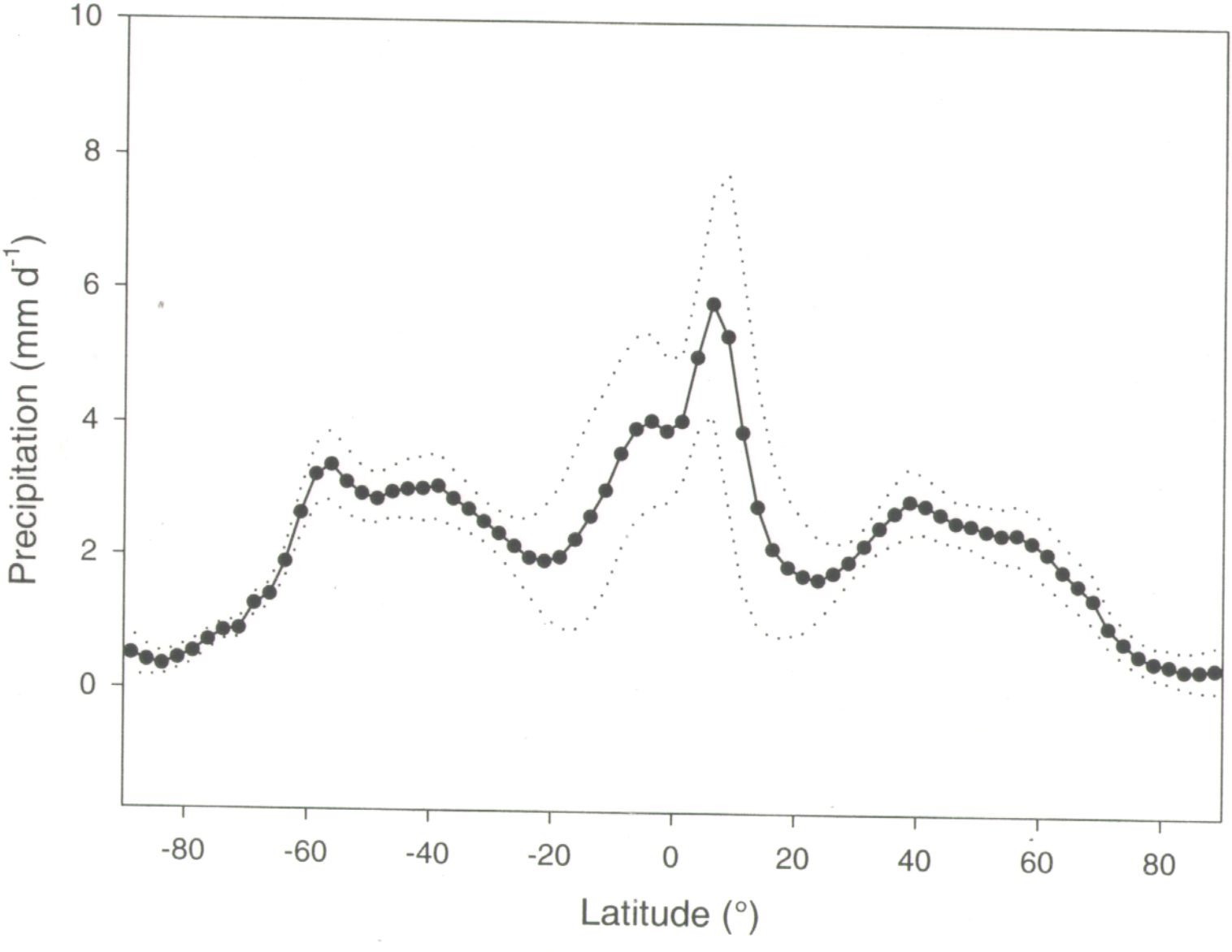
10
8
6
4
2
0
Precipitation (mm d-1)
-80
-60
-40
-20
0
20
40
60
80
Latitude (°)

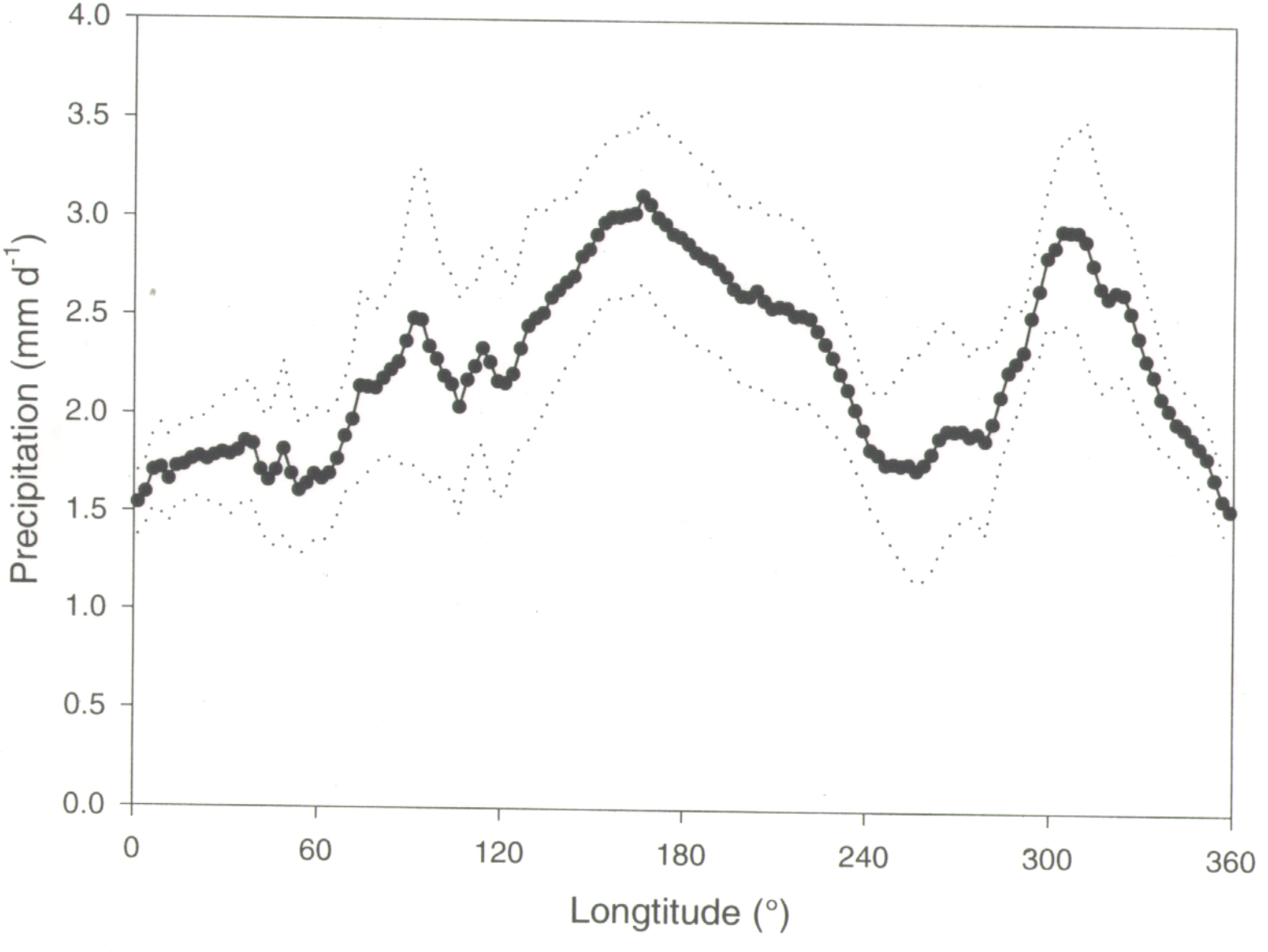
4.0
3.5
3.0
2.5
2.0
1.5
1.0
0.5
0.0
Precipitation (mm d-1)
0
60
120
180
240
300
360
Longtitude (°)

REPORT DOCUMENTION PAGE

Form Approved
OMB No. 0704-0188

1. AGENCY USE ONLY *(Leave blank)*	2. REPORT DATE	3. REPORT TYPE AND DATES COVERED
	2001	N/A

4. TITLE AND SUBTITLE

Seasonal Variation in Precipitation Patterns to the Global Ocean: An Analysis of the GPCP Version 2 Data Set

5. FUNDING NUMBERS

6. AUTHOR(S)

Jinchun Yuan and Richard Miller

7. PERFORMING ORGANIZATION NAME(S) AND ADDRESS(ES)

National Aeronautics and Space Administration
Earth Science Applications Directorate
John C. Stennis Space Center

8. PERFORMING ORGANIZATION REPORT NUMBER

SE-2001-06-00033-SSC

9. SPONSORING/MONITORING AGENCY NAME(S) AND ADDRESS(ES)

10. SPONSORING/MONITORING AGENCY REPORT NUMBER

11. SUPPLEMENTARY NOTES

N/A

12a. DISTRIBUTION/AVAILABILITY STATEMENT

Upon acceptance, this scientific paper will be available through the journal Global Biogoechemical Cycles, by interlibrary loan, or by requesting reprints from the author.

12b. DISTRIBUTION CODE

13. ABSTRACT *(Maximum 200 words)*

An analysis of temporal and spatial variation of oceanic precipitation was conducted on the GPCP version 2 data set. While the precipitation patterns observed are generally similar to the previous climatologies, new features and greater detail of global precipitation were revealed from our analysis of the GPCP data set. High precipitation was observed in the inter-tropical convergence zone, the South Pacific convergence zone, and the storm tracks in the North Pacific and Atlantic Oceans. Low precipitation was observed in the Polar regions and in the subtropics of the East Pacific, East Atlantic, and the Southeast and Northwest Indian Ocean. The spatial coverage of these high and low precipitation regions changed through the year. A strong seasonal cycle of precipitation was observed for the Northern and the Southern Hemispheres and for each ocean basin. Global precipitation also varied significantly with both latitude and longitude, with a latitudinal maximum at 56°S, 39°S, 4°S, 6°N, 39°N, and 56°N, and a longitudinal maximum over each ocean. The seasonal varying precipitation patterns are a foundation for evaluating the effect of wet deposition on ocean circulation, flux of chemical species, and its effect on marine ecosystems.

14. SUBJECT TERMS

Oceanic precipitation, global water cycle, air-sea interaction

15. NUMBER OF PAGES

32

16. PRICE CODE

17. SECURITY CLASSIFICATION OF REPORT	18. SECURITY CLASSIFICATION OF THIS PAGE	19. SECURITY CLASSIFICATION OF ABSTRACT	20. LIMITATION OF ABSTRACT
unclassified	unclassified	unclassified	